CRYSTAL GROWTH & DESIGN
2007
VOL. 7, NO. 8
1561−1564

Optical Floating Zone Growth of β-BaB_2O_4 from a $LiBa_2B_5O_{10}$-Based Solvent

Shilie Pan,[†] Jared P. Smit,[†] Courtney H. Lanier,[‡] Michael R. Marvel,[†] Laurence D. Marks,[‡] and Kenneth R. Poeppelmeier*[,†]

Department of Chemistry, Northwestern University, 2145 Sheridan Road, Evanston, Illinois 60208-3113, and Department of Materials Science and Engineering, Northwestern University, 2220 Campus Drive, Evanston, Illinois 60208-2500

Received March 7, 2007; Revised Manuscript Received May 15, 2007

ABSTRACT: Low-temperature barium metaborate β-BaB_2O_4 has been grown using a $LiBa_2B_5O_{10}$-based solvent in a four-mirror optical floating zone furnace with a traveling solvent zone configuration. The β-BaB_2O_4 rods grown are composed of several different crystal domains, ranging from 100 μm to 1 mm in diameter, and lithium, a component of the flux, was present only at the contaminant level. The technique demonstrates that thermal decomposition of the incongruently melting phase $LiBa_2B_5O_{10}$ can be used to grow β-BaB_2O_4.

Introduction

The study and crystal growth of low-temperature barium metaborate, β-BaB_2O_4 (β-BBO), have been important since the discovery of significant nonlinear optical properties in single crystals of β-BBO.[1,2] β-BBO crystals combine excellent linear and nonlinear optical characteristics: large effective second harmonic generation (SHG) coefficient, large birefringence, wide transparency region (190−3500 nm), high laser damage threshold, good mechanical properties, and low hygroscopicity. Because of these properties, β-BBO crystals are used in optoelectronics for laser frequency conversion (in particular, visible-to-UV frequency conversion) and although other nonlinear optical materials have been synthesized recently,[3−12] β-BBO remains of considerable value in optoelectronics.

Barium metaborate BaB_2O_4 exists in two modifications. The reversible phase transition from high-temperature α-BaB_2O_4 (α-BBO) to low temperature β-BBO has been described previously,[13] and its phase transition temperature is 925 °C.[14] Because of this phase transition, the growth of high-quality large single crystals is complicated. Additionally, the crystal growth of β-BBO is also difficult because the high viscosity of the β-BBO melt promotes glass formation.

The synthesis of single crystal β-BBO has been reported using various techniques such as the top-seeded solution growth technique, the laser-heated pedestal growth technique, the Czochralski technique, and other methods.[15−18] However, growing large high-quality single crystals of β-BBO remains a technologically sophisticated procedure.[19,20]

Growth in an optical floating zone furnace can produce crystals that are large in three dimensions from which large samples of specific orientations can be obtained. This technique has been employed successfully to grow other crystals.[21−27] Additionally, β-BBO crystal growth by the traveling solvent-zone melting method with a multicomponent Na_2O and B_2O_3 flux system has been attempted. However, flux inclusions were incorporated into the crystals.[28] In this paper, we present the crystal growth of β-BBO using a $LiBa_2B_5O_{10}$-based solvent with the optical floating zone furnace in the traveling solvent zone configuration.

Experimental Procedures

Feed and Support Rod Synthesis. The feed material β-BBO was prepared in air by calcining a 1:2 molar ratio of $BaCO_3$ (Alfa Aesar, 99.8% pure) and H_3BO_3 powder (Alfa Aesar, 99.99%) in a platinum crucible at 770 °C for 72 h. The experimental powder X-ray diffraction pattern of β-BBO is in agreement with the reported pattern.[29,30] The source of the solvent, $LiBa_2B_5O_{10}$, was synthesized by calcining Li_2CO_3 (Sigma Aldrich, 99%), $BaCO_3$ (Alfa Aesar, 99.8%), and H_3BO_3 powder (Alfa Aesar, 99.99%) in a 1:4:10 molar ratio at 700 °C for 48 h with several intermittent grindings. The experimental powder X-ray diffraction pattern of $LiBa_2B_5O_{10}$ is in agreement with the reported pattern.[31] It has been shown that the quality of the starting rods (for example, density and uniformity) directly influence the quality of the crystal grown in the optical floating zone furnace,[21,22] and in some cases poly(vinyl alcohol) binder is needed to facilitate the formation of high-quality rods. Therefore, 10 vol % aqueous poly(vinyl alcohol) (Alfa Aesar 98−99%, hydrolyzed low molecular weight) was added to both the β-BBO and the $LiBa_2B_5O_{10}$ powder to facilitate densification of the rods. The rods were formed by packing the powder with binder in a cylindrical rubber sleeve 6 mm in diameter by 60 mm long, which was then evacuated, sealed, and hydrostatically pressed at 70 MPa for 2 h. To form dense polycrystalline rods, the packed and pressed rods were sintered in air. The resulting rod density was 3.25 g/cm^3 (compared to a crystal density of 3.86 g/cm^3), which is near the minimum density requirement for crystal growth of β-BBO in the optical floating zone furnace. The β-BBO feed rod was sintered at 840 °C for 48 h, and the $LiBa_2B_5O_{10}$ support rod was sintered at 760 °C for 72 h.

Initially, the β-BBO feed rod was heated at a rate of 10 °C /min from room temperature to 840 °C in air for 48 h. However, the resultant rod was crooked and severely cracked (the top rod in Figure 1). When the temperature was raised to 500 °C at a rate of 0.1 °C/min and held for 48 h to burn the poly(vinyl alcohol) gradually and thoroughly, and then raised to 840 °C at a rate of 0.1 °C/min and held, the resultant rod was very straight and not cracked (the bottom rod in Figure 1).

Crystal Growth. The feed rod was suspended from the upper shaft of the floating zone furnace using a platinum wire, while the support rod was affixed rigidly to the bottom shaft using steel wire. Growth was carried out in an optical image furnace (CSI FZ-T-10000-H-VI-VP, Crystal Systems, Inc.; Japan) equipped with four 300 W tungsten halide lamps focused by four polished elliptical mirrors shown in Figure S1 in Supporting Information.

Crystal Characterization. Phase identification was made using both crystal and powder X-ray diffraction (PXRD). PXRD analysis of ground crystals of β-BBO was performed at room temperature in the angular range of $2\theta = 10-70°$ with a scan step width of 0.02° and a fixed

* To whom correspondence should be addressed. Phone: (847) 491-3505. Fax: (847) 491-7713. E-mail: krp@northwestern.edu.
[†] Department of Chemistry, Northwestern University.
[‡] Department of Materials Science and Engineering, Northwestern University.

10.1021/cg0702232 CCC: $37.00
Published on Web 06/27/2007

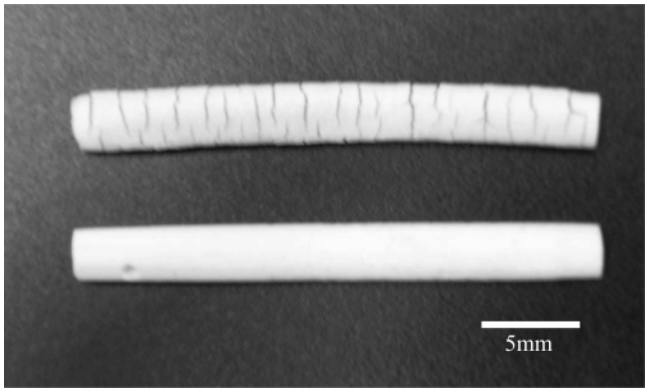

Figure 1. Pure β-BBO feed rod at different heating rates. The top β-BBO rod is at a rate of 10 °C/min from room temperature to 840 °C; the bottom β-BBO rod is at a rate of 0.1 °C/min from room temperature to 840 °C.

counting time of 1 s/step using an automated Rigaku X-ray diffractometer equipped with a diffracted-beamed monochromator set for Cu $K\alpha$ ($\lambda = 1.5418$ Å) radiation and a nickel filter.

Single crystal measurements were made on a Bruker SMART 1000 CCD diffractometer using monochromatic Mo Kα radiation ($\lambda = 0.71073$ Å) and integrated with the SAINT Plus program at a temperature of −120 °C.[32] A single crystal was mounted on a glass fiber for study by single-crystal X-ray diffraction, and all calculations were performed with programs from the SHELXTL crystallographic software package.[33]

The composition and microstructure of the β-BBO crystals were characterized by scanning electron microscopy (SEM) and secondary ion mass spectroscopy (SIMS). Both the crystal quality and the chemical uniformity were examined. Cross sectional disks were sliced perpendicular to the growth direction from the grown β-BBO rod with a wire saw, and the disks were polished with silicon carbide paper to create a smooth surface. No further preparations were necessary for SIMS; however, prior to SEM analysis the sample was coated with a 4.0 nm layer of Au/Pd to increase secondary electron emission and prevent charging. SEM was performed with a Hitachi S-3500 microscope operating at 20 kV, and SIMS was performed with a PHI-TRIFT III instrument using 15 keV Ga^+ ions. Area spectra and composition maps were obtained under positive ion mode, thus measuring the cation composition of the sample.

Results and Discussion

Successful crystal growth involves a stable liquid zone. In the optical floating zone furnace, crystal growth begins by melting the top of the support rod and connecting a counter-rotating feed rod, thereby forming a liquid zone between the counter-rotating rods. Achieving a stable liquid zone requires dense, chemically homogeneous, straight, and precisely aligned feed and support rods. If the starting feed rod is not adequately dense, then more liquid can crystallize than will be replenished from the melting feed rod or the liquid can penetrate into the feed rod by capillary action. In either situation, the diminishing volume of liquid will cause the feed rod to disconnect from the support rod. Additionally, crooked or imprecisely aligned rods rotate out of the center axis during crystal growth and disturb the stability of the liquid zone.

Because BBO has a phase transition at 925 °C, β-BBO crystals can be grown from solutions to avoid the $\alpha-\beta$ solid-state phase transformation encountered when crystals are grown directly from the melt.[19,20] To find a suitable solvent for use in an optical floating zone furnace, several additional considerations were taken into account compared to a flux assisted growth in a crucible. First, the solute and solvent must form a liquid phase with enough surface tension to sustain a molten floating zone between the two rods during the growth process.[21,22] Preferably the solvent should not penetrate deeply into the feed rod by capillary action along grain boundaries, thereby causing an unstable growth condition. In addition, the solvent chosen must have a low vapor pressure in the liquid-phase such that it will not evaporate during the course of the growth. If the solvent selected was volatile and it evaporated during the course of the growth, then the liquid composition would change and affect the dynamic equilibrium needed for continuous growth of a crystal of constant composition. Other growth attempts using PbF_2-B_2O_3, BaF_2, PbO, and Na_2O[16,34−37]-based solvents failed because of severe penetration, solvent volatility, or an unstable molten zone.

In the current work, a β-BBO crystal rod was grown (Figure 2) using a $LiBa_2B_5O_{10}$-based solvent that serves to both lower the temperature and prevent the phase transition. According to the phase diagram represented in Figure 3, the binary BaB_2O_4−$Li_2B_2O_4$ system[38] contains the compound $LiBa_2B_5O_{10}$ that undergoes a peritectic reaction at 930 °C and decomposes into α-BBO and liquid. However, as discussed in a later section, β-BBO is obtained rather than α-BBO. Relating to crystal growth in the traveling solvent zone furnace, this means that once the top of the support rod is fully melted, β-BBO will

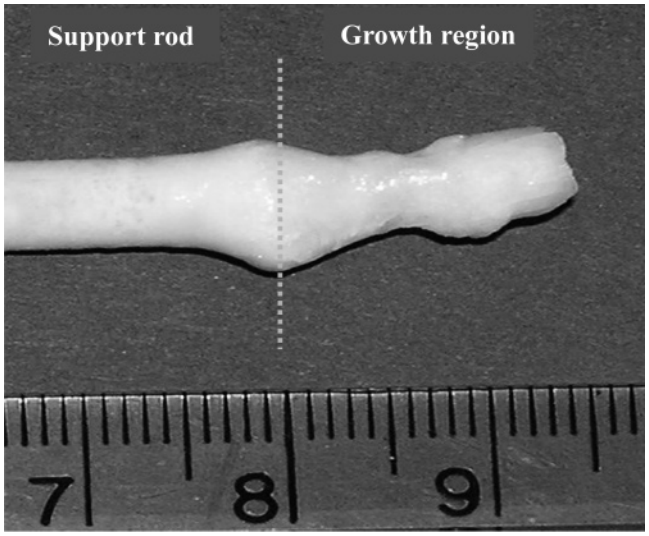

Figure 2. Synthetic β-BBO rod grown using a $LiBa_2B_5O_{10}$-based solvent. Each line represents 1 mm. The $LiBa_2B_5O_{10}$ support rod is on the left-hand side, and the growth region is to the right. The dashed line separates the region of the crystal used for SEM and SIMS analysis.

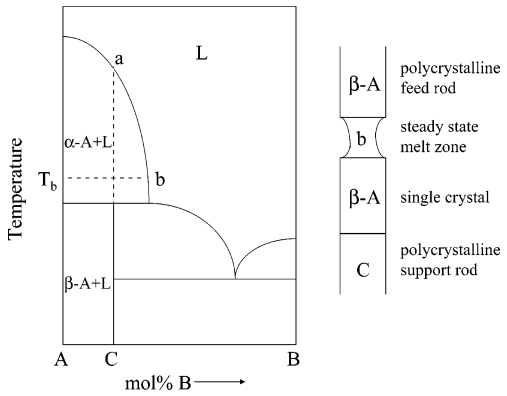

Figure 3. Schematic view of BaB_2O_4 crystal growth from the $LiBa_2B_5O_{10}$-based solvent. Keeping with the special notation used in describing these oxide systems, A denotes BaB_2O_4, B denotes $Li_2B_2O_4$, C denotes $LiBa_2B_5O_{10}$, α-A denotes α-BaB_2O_4, β-A denotes β-BaB_2O_4, and L denotes liquid.

Table 1. Crystal Data and Structure Refinement for BaB_2O_4

empirical formula	BaB_2O_4
wavelength	0.71073 Å
formula weight	222.96
crystal system	trigonal
space group, Z	$R3c$, 6
unit cell dimensions	$a = 8.3824(3)$ Å $\alpha = 96.86°$
density (calculated)	3.862 g/cm^3
absorption coefficient	10.215 /mm
crystal size	$0.1 \times 0.2 \times 0.2$ mm^3
theta range for data collection	3.7− 28.81°
refinement method	full-matrix least-squares on F^2
goodness-of-fit on F^2	1.025
final R indices [$I > 2\sigma(I)$][a]	$R_1 = 0.0209$, $wR_2 = 0.0516$
R indices (all data)[a]	$R_1 = 0.0214$, $wR_2 = 0.0518$
largest diff peak and hole	1.247 and −1.003 e Å^{-3}

[a] $R_1 = \sum||F_o| - |F_c||/\sum|F_o|$ and $wR_2 = [\sum w(F_o^2 - F_c^2)^2/\sum wF_o^4]^{1/2}$ for $F_o^2 > 2\sigma(F_o^2)$.

nucleate onto the support rod. β-BBO is precipitated from the melt, and therefore to prevent zone leveling[39] from occurring (in which the equilibrium would continue down the liquidus line to the peritectic point and establish a Li-rich steady-state melt composition thereby depositing solid $LiBa_2B_5O_{10}$), β-BBO needs to be replenished via the feed rod to maintain a constant Ba-rich liquid composition. This is analogous to the "push−pull" method of single-crystal growth developed by Nelson for growth of germanium,[40] by which the liquid composition is held constant by continuously adding material (of the same composition) as the growing rod. If the equilibrium liquid composition at the solidification front remains Ba-rich, then only β-BBO will be deposited. Note that this procedure is different from the case of other peritectic systems in which zone leveling and deposition of the incongruently melting phase are desired. In the case of growth of $Mg_3(VO_4)_2$[21] and high T_c cuprates,[23] for example, both the support (or solvent disk, as the case may be) and the feed rods are composed of the incongruently melting material, and in these cases, zone leveling occurs, and after a brief period in which "the first grown material" is deposited, crystallization of the incongruently melting phase commences. In fact, the optical floating zone furnace in the traveling solvent zone configuration in general utilizes such peritectic phase transitions to grow single crystals of incongruently melting materials.

The crystal growth commences with β-BBO crystallization on top of the support rod and proceeds with the upward translation of the mirror stage. The liquid composition changes continuously until a steady state is established between the liquid and the crystallized β-BBO. After the steady state of the molten zone is formed, the β-BBO phase travels through a lithium-based flux and is grown out of the flux, and the grains are aligned across the volume of the growth region. The crystallized β-BBO is replenished in the liquid zone from the feed rod, and therefore continuous growth of crystalline β-BBO is maintained. The growth rate and speed of the counter-rotating support and feed rods were varied to minimize the number of crystal domains, and the growth rate adopted was 0.3 mm/h. Faster rates resulted in flux inclusions.

As mentioned, although the phase diagram suggests that α-BBO should crystallize from the flux, PXRD of the ground crystals is in agreement with the reported results,[29,30] which shows that the product is β-BBO. Additionally, single-crystal X-ray data (Table 1) were refined and agree with previously published structures of the low-temperature phase in the $R3c$ space group.[29,30] The final R1 and wR2 values are 0.02 and 0.05 for all data, respectively, and final atomic coordinates and equivalent isotropic displacement parameters of β-BBO are listed in Table 2.

Table 2. Atomic Coordinates ($\times 10^4$) and Equivalent Isotropic Displacement Parameters (Å$^2 \times 10^3$) for BaB_2O_4[a]

atom	Wyckoff position	x	y	z	U_{eq}
Ba(1)	6b	3892(1)	333(1)	7530(1)	8(1)
B(1)	6b	6310(7)	7747(7)	8560(6)	10(1)
B(2)	6b	586(7)	1022(7)	8849(7)	11(1)
O(1)	6b	6577(5)	8751(4)	7347(4)	14(1)
O(2)	6b	6066(4)	2710(5)	6854(5)	13(1)
O(3)	6b	2921(4)	91(4)	4399(4)	11(1)
O(4)	6b	1378(4)	9725(5)	9309(5)	16(1)

[a] U_{eq} is defined as one-third of the trace of the orthogonalized U_{ij} tensor.

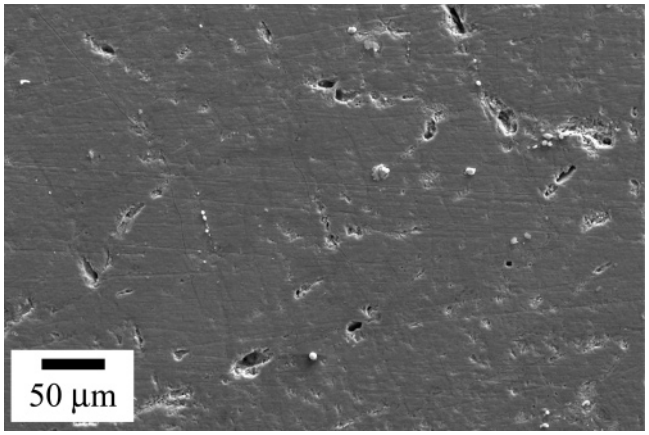

Figure 4. SEM micrograph from β-BBO cross section.

β-BBO directly crystallizes from the molten zone rather than α-BBO, which is predicted from the phase diagram in Figure 3. Therefore, the crystallization of β-BBO from the flux is likely a metastable crystal growth process. Metastable crystallization is explained by the Ostwald step rule,[41] which suggests that a metastable, low-temperature phase crystallizes at temperatures above the phase transition point before the stable, high-temperature phase appears, when the liquid is supercooled. Supercooling often occurs from viscous melts, and borate melts are highly viscous in general. The Ostwald step rule is also supported by other studies[17,18,42] and is the likely reason why metastable β-BBO was obtained from a $LiBa_2B_5O_{10}$-based solvent.

The resulting rod was 15 mm long and 3 mm in diameter. SEM and optical microscopy analysis of the rod cross-section indicated that the rod was composed of several different crystal domains, ranging from 100 μm to 1 mm in diameter. The morphology and stoichiometry of the grains were uniform across the disk. Figure 4 shows an SEM micrograph of a polished cross-section of the β-BBO rod showing small holes (typically less than 25 μm) contained in the crystal. These holes develop during the growth process and are frozen in upon rapid cooling of the molten zone.

SIMS was used to test for the compositional uniformity of the β-BBO crystal as well as ensure that no lithium remained in the structure owing to the $LiBa_2B_5O_{10}$ solvent-based growth. Cross sectional disk samples were sputtered in situ prior to analysis to remove any surface-adsorbed contaminants. Positive ion mode chemical maps showed a uniform distribution of barium and boron across the disk (Figure S4, Supporting Information). Low levels of tramp impurities (owing to the impurity of the starting materials) were uniformly detected, namely, Na and K. Li was also present uniformly in the polycrystalline, but it was measured to be at the same level as the tramp impurities. An independent SIMS analysis of a

$LiBa_2B_5O_{10}$ sample indicated a peak ratio for Li to B of 57:1, and the ratio for our grown β-BBO crystal was 0.6:1. Therefore, the SIMS analysis suggests that not only did the β-BBO crystal have a uniform composition, but also the $LiBa_2B_5O_{10}$ solvent did not significantly contaminate the crystal with lithium during growth.

Conclusions

A rod of β-BaB_2O_4 was grown by the optical floating zone method in the traveling solvent zone configuration using a $LiBaB_5O_{10}$-based solvent. The β-BaB_2O_4 rods grown are composed of several different crystal domains, ranging from 100 μm to 1 mm in diameter, and lithium, a component of the flux system used in the growth, is present only at the contaminant level.

It should be noted that using the optical floating zone furnace in the traveling solvent zone configuration with this type of flux system is a new methodology for growing crystals of β-BBO. Unique to the growth of β-BBO, we used a peritectic reaction to our benefit in thermally decomposing an incongruently melting phase to grow an entirely different phase.

Acknowledgment. The authors thank Charlotte L. Stern for assistance with crystallographic measurements. The authors gratefully acknowledge the financial support from the National Science Foundation (Solid-State Chemistry Award No. DMR-0312136 and DMR-0604454) and the use of the Central Facilities supported by the MRSEC program of the National Science Foundation (DMR-0520513) at the Materials Research Center of Northwestern University. The SEM studies were performed in the EPIC facility of NUANCE Center at Northwestern University. The SIMS work was performed in the Keck-II facility of NUANCE Center at Northwestern University. NUANCE Center is supported by the NSF-NSEC, NSF-MRSEC, Keck foundation, the State of Illinois, and Northwestern University.

Supporting Information Available: Photographs of the optical floating zone furnace, calculated and observed X-ray diffraction pattern data, SIMS composition maps, and an X-ray crystallographic file in CIF format including crystallographic details, interatomic distances, and angles for β-BBO. This material is available free of charge via the Internet at http://pubs.acs.org.

References

(1) Chen, C.; Wu, B.; Jiang, A.; You, G. *Sci. Sin.* **1985**, *B28*, 235.
(2) Chen, C.; Liu, G. *Annu. Rev. Mater. Sci.* **1986**, *16*, 203.
(3) Chen, C.; Wu, Y.; Jiang, A.; You, G.; Li, R.; Lin, S. *J. Opt. Soc. Am.* **1989**, *B6*, 616.
(4) Wu, Y.; Sasaki, T.; Nakai, S.; Yokotani, A.; Tang, H.; Chen, C. *Appl. Phys. Lett.* **1993**, *62*, 2614.
(5) Chen, C.; Xu, Z.; Deng, D.; Zhang, J.; Wong, G. K. L.; Wu, B.; Ye, N.; Tang, D. *Appl. Phys. Lett.* **1996**, *68*, 2930.
(6) Chen, C.; Wang, Y.; Wu, B.; Wu, K.; Zeng, W.; Yu, L. *Nature* **1995**, *373*, 322.
(7) Mori, Y.; Kuroda, I.; Nakajima, S.; Sasaki, T.; Nakai, S. *Appl. Phys. Lett.* **1995**, *67*, 1818.
(8) Aka, G.; Kahn-Harari, A.; Vivien, D.; Benitez, J.-M.; Salin, F.; Godard, J. *Eur. J. Solid State Inorg. Chem.* **1996**, *33*, 727.
(9) Wu, Y.; Liu, J.; Fu, P.; Wang, J.; Zhou, H.; Wang, G.; Chen, C. *Chem. Mater.* **2001**, *13*, 753.
(10) Pan, S.; Wu, Y.; Fu, P.; Zhang, G.; Li, Z.; Du, C.; Chen, C. *Chem. Mater.* **2003**, *15*, 2218.
(11) Pan, S.; Wu, Y.; Fu, P.; Wang, X.; Zhang, G.; Chen, C. *J. Opt. Soc. Am.* **2004**, *B21*, 761.
(12) Zumsteg, F. C.; Bierlein, J. D.; Gier, T. E. *J. Appl. Phys.* **1976**, *47*, 4980.
(13) Levin, E. M.; McMurdie, H. F. *J. Am. Ceram. Soc*. **1949**, 32, 99.
(14) Hübner, K. H. *Neues Jahrb. Mineral. Monatsh*. **1969**, *8*, 335.
(15) Jiang, A.; Cheng, F.; Lin, Q.; Cheng, Z.; Zheng, Y. *J. Cryst. Growth* **1986**, *79*, 963.
(16) Tang, D.; Route, R. K.; Feigelson, R. S. *J. Cryst. Growth* **1988**, *91*, 81.
(17) Itoh, K.; Marumo, F.; Kuwano, Y. *J. Cryst. Growth* **1990**, *106*, 728.
(18) Kouta, H.; Kuwano, Y.; Itoh, K.; Marumo, F. *J. Cryst. Growth* **1991**, *114*, 676.
(19) Hong, X.; Lu, K.; Li, L.; Tang, D. *J. Cryst. Growth* **1998**, *193*, 610.
(20) Xu, Z. *J. Cryst. Growth* **2004**, *265*, 553.
(21) Pless, J. D.; Erdman, N.; Ko, D.; Marks, L. D.; Stair, P. C.; Poeppelmeier, K. R. *Cryst. Growth Des.* **2003**, *3*, 615.
(22) Chiaramonti, A. N.; Pless, J. D.; Liu, L.; Smit, J. P.; Lanier, C. H.; Poeppelmeier, K. R.; Stair, P. C.; Marks, L. D. *Cryst. Growth Des.* **2004**, *4*, 749.
(23) Revcolevschi, A.; Jegoudez, J. *Prog. Mater. Sci.* **1997**, *42*, 321.
(24) Guptasarma, P.; Williamsen, M. S.; Sarma, B. K.; Suslov, A.; Schneider, M. L.; Sendelbach, S.; Onellion, M.; Taft, G. *J. Phys. Chem. Solids* **2006**, *67*, 525.
(25) Pucher, K.; Hemberger, J.; Mayr, F.; Fritsch, V.; Loidl, A.; Scheidt, E. W.; Klimm, S.; Horny, R.; Horn, S.; Ebbinghaus, S. G.; Reller, A.; Cava, R. J. *Phys. Rev. B* **2002**, *65*, 104523/1.
(26) Abbamonte, P.; Blumberg, G.; Rusydi, A.; Gozar, A.; Evans, P. G.; Siegrist, T.; Venema, L.; Eisaki, H.; Isaacs, E. D.; Sawatzky, G. A. *Nature* **2004**, *431*, 1078.
(27) Kimura, T.; Lawes, G.; Goto, T.; Tokura, Y.; Ramirez, A. P. *Phys. Rev. B* **2005**, *71*, 224425/1.
(28) Hengel, R. O.; Fischer, F. *J. Cryst. Growth* **1991**, *114*, 656.
(29) Liebertz, J.; Stahr, S. *Z. Kristallogr.* **1983**, *165*, 91.
(30) Frohlich, R. *Z. Kristallogr.* **1984**, *168*, 109.
(31) Smith, R. W.; Keszler, D. A. *Mater. Res. Bull.* **1989**, *24*, 725.
(32) SAINT Plus, version 6.02A; Bruker Analytical X-ray Instruments, Inc.: Madison, WI, 2000.
(33) Sheldrick, G. M. *SHELXTL*, Version 6.14; Bruker Analytical X-ray Instruments, Inc.: Madison, WI, 2003.
(34) Tang, D. Y.; Zeng, W. R.; Zhao, Q. L. *J. Cryst. Growth* **1992**, *123*, 445.
(35) Bordui, P. F.; Calvert, G. D.; Blachman, R. *J. Cryst. Growth* **1993**, *129*, 371.
(36) Feigelson, R. S.; Raymakers, R. J.; Route, R. K. *J. Cryst. Growth* **1989**, *97*, 352.
(37) Cheng, L. K.; Bosenberg, W.; Tang, C. L. *Prog. Cryst. Growth Charact.* **1990**, *20*, 9.
(38) Huang, Q. Z.; Wang, G. F.; Liang, J. K. *Wuli Xuebao* **1984**, *33*, 76.
(39) Pfann, W. G. *Zone Melting*, 2nd ed.; John Wiley and Sons: New York, 1966.
(40) Nelson, H. *Transistors I*; RCA Laboratories: Princeton, NJ, 1956.
(41) Ostwald, W. *Z. Phys. Chem.* **1897**, *22*, 289.
(42) Kozuki, Y.; Itoh, M. *J. Cryst. Growth* **1991**, *114*, 683.

CG0702232